Appl. Phys. A 29, 9–18 (1982)

Applied Physics A Solids and Surfaces

Periodic Surface Structures Frozen into CO_2 Laser-Melted Quartz

F. Keilmann and Y. H. Bai*

Max-Planck-Institut für Festkörperforschung, D-7000 Stuttgart 80, Fed. Rep. Germany

Received 13 April 1982/Accepted 3 May 1982

Abstract. Ripple formation on laser-treated surfaces is studied in the infrared Reststrahlen region of quartz. We observe, for the first time, a dispersive behaviour of the ripple period. Thus we are led to a new explanation of the ripples: they represent holographic recordings of propagating electromagnetic surface waves (surface polaritons). Basic to this effect is a – hitherto not described – interference between a plane and an inhomogeneous wave, offering new possibilities for surface polariton physics.

PACS: 42.40, 42.82, 71.36, 73.90

Laser treatment can impress spatially periodic microscopic structures on the surface of many materials including metals and semiconductors. In several cases it has been clearly demonstrated that the structures consist of elevated and depressed regions which led to the name surface ripple. The ripple period was found in [1–8] to be nearly equal to the laser wavelength at normal incidence ($\alpha = 0°$), and to vary approximately as $(1 + \sin\alpha)$ otherwise [2–8]. This suggested that the effect is due to interference of the incident and a scattered field, the latter arising from disturbances at the surface. We agree with this view, and while [4] and [9] discuss the near field around specific scattering centers we stress here that the scattered fields effective in ripple formation are essentially those of the well-known surface polaritons, i.e. of electromagnetic modes bound to and propagating along the surface.

In our experiment the frequency is varied within a resonant absorption region of quartz. Therefore, the surface polariton phase velocity changes with frequency, and as we expect, we find the ripple period to scale nonlinearly with the incident (vacuum) wavelength. Previously Isenor [5] observed a slightly nonlinear relation in the case of NiP which we suggest can be explained by surface plasmon polariton dispersion.

Usually [2, 4–7] the surface ripple orientation is observed to depend on the direction of polarization of the incident light rather than on the crystallographic orientation of the solid. This is expected if surface waves play a role. Since surface polaritons are TM polarized, one expects orthogonal orientation of the driving electric field and the ripple lines. This is, in fact, observed in [2, 4–7] and in our work. In addition, however, we find a spectral region where TE modes coexist or even dominate.

Time-resolved reflection [10] can be used to study the dynamics of ripple formation. In this work, however, we will not try to answer the question of how the initially plane surface deforms during the melting and resolidification phases once a temperature grating is present due to a partially standing electromagnetic wave.

On the other hand, we notice a strong feedback effect in the polariton model of ripple generation. The ripples initially form according to the phase velocity of polaritons on a plane surface. This velocity then changes on appearance of the ripples. Our experiment indicates a considerable shift of the surface polariton dispersion curves due to this feedback effect.

For completeness we reference two papers on mechanisms of ripple generation which do not involve surface polaritons. One deals with structures produced on oxide coated Si [11] and is interpreted in terms of

* Permanent address: Institute of Acoustics, Academia Sinica, Beijing, China

0721-7250/82/0029/0009/$02.00

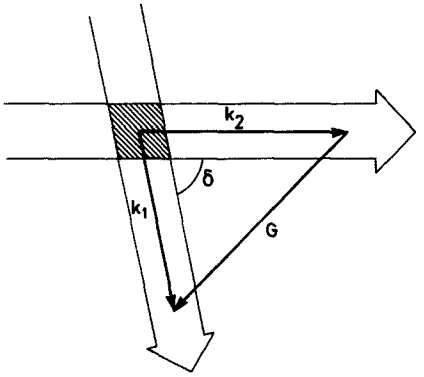

Fig. 1. Orientation of interference fringes produced by two plane waves with wavevectors $\mathbf{k}_1$ and $\mathbf{k}_2$

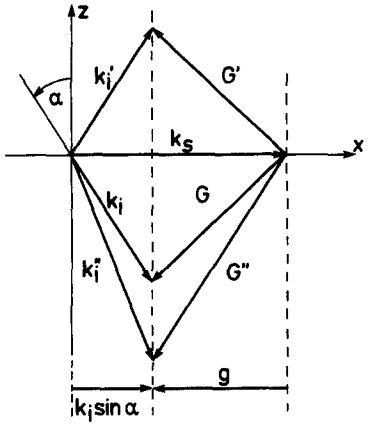

Fig. 2. Interference grating vectors $\mathbf{G}=\mathbf{k}_s-\mathbf{k}_i$ from a surface wave propagating along x and an obliquely incident (as well as reflected and refracted) plane wave

differential thermal expansion of these materials. The other effect [12] invokes the action of standing surface acoustic waves on GaAs driven at the beat frequencies of the multimode ruby laser used.

1. Surface Polariton Interference

Wavefronts and strength of the electric field connected to a surface polariton can be made visible by interference. Surprisingly, this effect has to our knowledge not been described in the literature. Much as in usual holography a reference electric field can be superimposed to generate an interference pattern which is recorded in a suitable photographic medium. In the case of laser generated surface ripples the reference field is that of the incident (and reflected) laser beam, while the thermal deformability of the material's surface serves as the recording medium.

The interference pattern formed by two waves of the same frequency can be easily found by wave vector subtraction. Assuming the waves to be given by $\mathbf{E}_1\exp[\mathrm{i}(\mathbf{k}_1\mathbf{r}-\omega t)]$ and $\mathbf{E}_2\exp[\mathrm{i}(\mathbf{k}_2\mathbf{r}-\omega t)]$, respectively, we obtain the time-averaged intensity to be $I=\mathbf{E}_1^2+\mathbf{E}_2^2+2\mathbf{E}_1\mathbf{E}_2\cdot\cos[(\mathbf{k}_1-\mathbf{k}_2)\mathbf{r}]$. The interference "grating" wavevector $\mathbf{G}=\mathbf{k}_1-\mathbf{k}_2$ is normal to the surfaces of maximum intensity, and $d=2\pi\,|\mathbf{G}|^{-1}$ is the fringe separation. For plane waves travelling in a medium of refractive index n and intersecting at an angle δ (Fig. 1) the maxima or minima surfaces are planes with $d=\lambda_{\mathrm{vac}}[2n\sin(\delta/2)]^{-1}$.

Consider now surface polaritons [13–15] bound to the interface $z=0$ between vacuum ($z>0$) and a solid ($z<0$). The electric field is maximum at $z=0$ and decays as $\exp(-k_V z)$ into the vacuum and as $\exp(-k_M|z|)$ into the medium with k_V, k_M real. The propagation vector $\mathbf{k}_s$ of the surface polariton is thus confined to the $x-y$ plane of the surface. Assume now $\mathbf{k}_s$ in the positive x-direction. Furthermore assume an incident plane wave of wavevector $\mathbf{k}_i$ inclined at angle α in the $x-z$ plane (Fig. 2). The resulting interference pattern is described by the grating wavevector $\mathbf{G}$ for the vacuum side. Two other interference gratings exist, characterized by $\mathbf{G}'$ and $\mathbf{G}''$, due to the reflected wave $\mathbf{k}_i'$ in vacuum, and due to the refracted wave $\mathbf{k}_i''$ in the medium, respectively. Since we are interested only in surface patterns we need only consider components of $\mathbf{G}$ in the $x-y$ plane. The conclusion is very simple: a single grating wavevector $\mathbf{g}$ parallel to x results for all the incident, reflected and refracted reference waves, with the fringe separation $d=2\pi\,|\mathbf{g}|^{-1}=2\pi(|\mathbf{k}_i|\sin\alpha-|\mathbf{k}_s|)^{-1}$. Inserting the vacuum wavelength $\lambda_{\mathrm{vac}}=2\pi|\mathbf{k}_i|^{-1}$ and the phase velocity of the surface polariton $v_{\mathrm{ph}}=c|\mathbf{k}_i|\,|\mathbf{k}_s|^{-1}$ we obtain

$$d=\lambda_{\mathrm{vac}}/(c/v_{\mathrm{ph}}-\sin\alpha)\,. \tag{1}$$

Let us also consider the more general case of a surface polariton propagating not parallel to the plane of incidence ($x-z$). For simplicity, we assume an isotropic material so that the surface polariton wavevectors form a circle in the $x-y$ plane (Fig. 3). Except for polaritons propagating in the plane of incidence the interference fringes no longer come out to be perpendicular to either the polariton propagation direction or to the plane of incidence. The fringe separation is now

$$d=\lambda_{\mathrm{vac}}\left[\left(\frac{c}{v_{\mathrm{ph}}}\cos\beta-\sin\alpha\right)^2+\left(\frac{c}{v_{\mathrm{ph}}}\sin\beta\right)^2\right]^{-1/2}. \tag{2}$$

As long as $v_{\mathrm{ph}}\lesssim c$ this is very nearly the equation of an ellipse with eccentricity

$$\eta=(v_{\mathrm{ph}}/c)\sin\alpha\,. \tag{3}$$

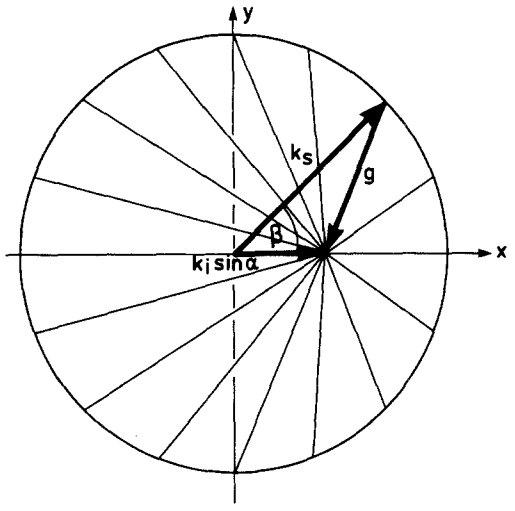

Fig. 3. Interference grating from a surface wave propagating outside the $x-z$ plane of incidence of a plane wave

2. Mechanisms of Surface Polariton Generation

Surface polaritons can be effectively launched from an incident plane wave by suitable phase matching techniques, e.g. using prism [16, 17] or grating [18] couplers. In the case of laser surface ripple generation, however, we think that microscopic disturbances serve as primary, localized sources of surface polaritons. Fine scratches are expected to act as line sources while small dust particles might emit circular waves. The amplitude of these waves will vary with direction for a linearly polarized driving field, since surface polaritons are strongly polarized, having no transverse electric field component in the surface plane. Maximum amplitude is therefore expected for polaritons propagating in the direction of the driving electric field. The maximum interference contrast is also expected for just this situation.

Once a small ripple structure has formed on the surface it acts itself as an antenna, coupling the incident beam to the surface wave. This coupling is phase-matched because the same vector diagram applies for "grating coupling" [18] as for the formation of the interference pattern (Fig. 3). Note therefore that this self-amplifying system is remarkably adaptive: if with increasing ripple depth there occurs a change of the surface wave dispersion, i.e. of v_{ph}, the ripple period also changes according to (2). This behaviour can be viewed as a space-domain analog of frequency-pulling in lasers [19, 20].

3. Experiment

Our laser ripple studies began with accidental observations of damage on quartz by a TEA CO_2 laser. The pulse has an energy of a few J and a length of 80 ns (FWHM) followed by tail of about 100 ns. The frequency is controlled by an internal grating. While many longitudinal modes (spaced 46 MHz) produce a spiky temporal shape, the transverse intensity distribution is nearly that of a fundamental mode with a spot diameter near 2 cm. This pulse causes plasma production, melting and damage on many materials. On quartz and glass for example, a bright plasma region is seen extending a few mm away from the surface.

It is fortuitous that a Reststrahlen vibrational absorption region of quartz [21] and quartz glass [22] overlaps the tuning range 930–1080 cm^{-1} of the CO_2 laser. Thus dispersion effects in ripple formation can be studied. In our experiments we used flat optically polished samples of quartz and Suprasil (product of Heraeus, Hanau). Usually the laser was attenuated to near the plasma formation threshold. The exposed samples were inspected in a phase contrast microscope.

4. Results

After a small number of shots (3 s apart) isolated wavetrains appear (Fig. 4a and b) at many locations within the laser damage area, sometimes starting from an identificable scratch or dust grain. The length of these wavetrains is of the order of 100 μm in each direction. Such isolated wavetrains coalesce after further shots into a grating pattern covering the entire central region of the laser spot (Fig. 4c). Dark zones separate regions where an additional fringe is fitted in, resembling an edge dislocation in a crystal. A magnified view of this pattern is presented in Fig. 5, which indicates a roughly sinusoidal shape of the grooves.

For a determination of the average fringe distance of patterns such as in Fig. 4c we measured the angles of diffraction of normally incident He–Ne laser light at a wavelength of 0.6328 μm. Furthermore, the measurement of the first- and second-order diffracted intensities I_1 and I_2 gives a relative measure of the average form of the ripple. Figure 6 shows that for conditions as in Figs. 4 and 5 the first-order diffraction efficiency increases exponentially with the number of shots and saturates at $I_1/I_0 \simeq 1\%$. The rise of the relative efficiency I_2/I_2 of the second-order diffraction indicates an increasing distortion of the initially quite sinusoidal groove shape. Furthermore we see in Fig. 6 that the ripple pattern can be erased by further shots of orthogonal polarization, while a new ripple pattern with orthogonal orientation builds up. Microscopic inspection shows no spatial overlap of both structures, the new one develops from the center of the laser spot while the former stays longest at the low-intensity boundary.

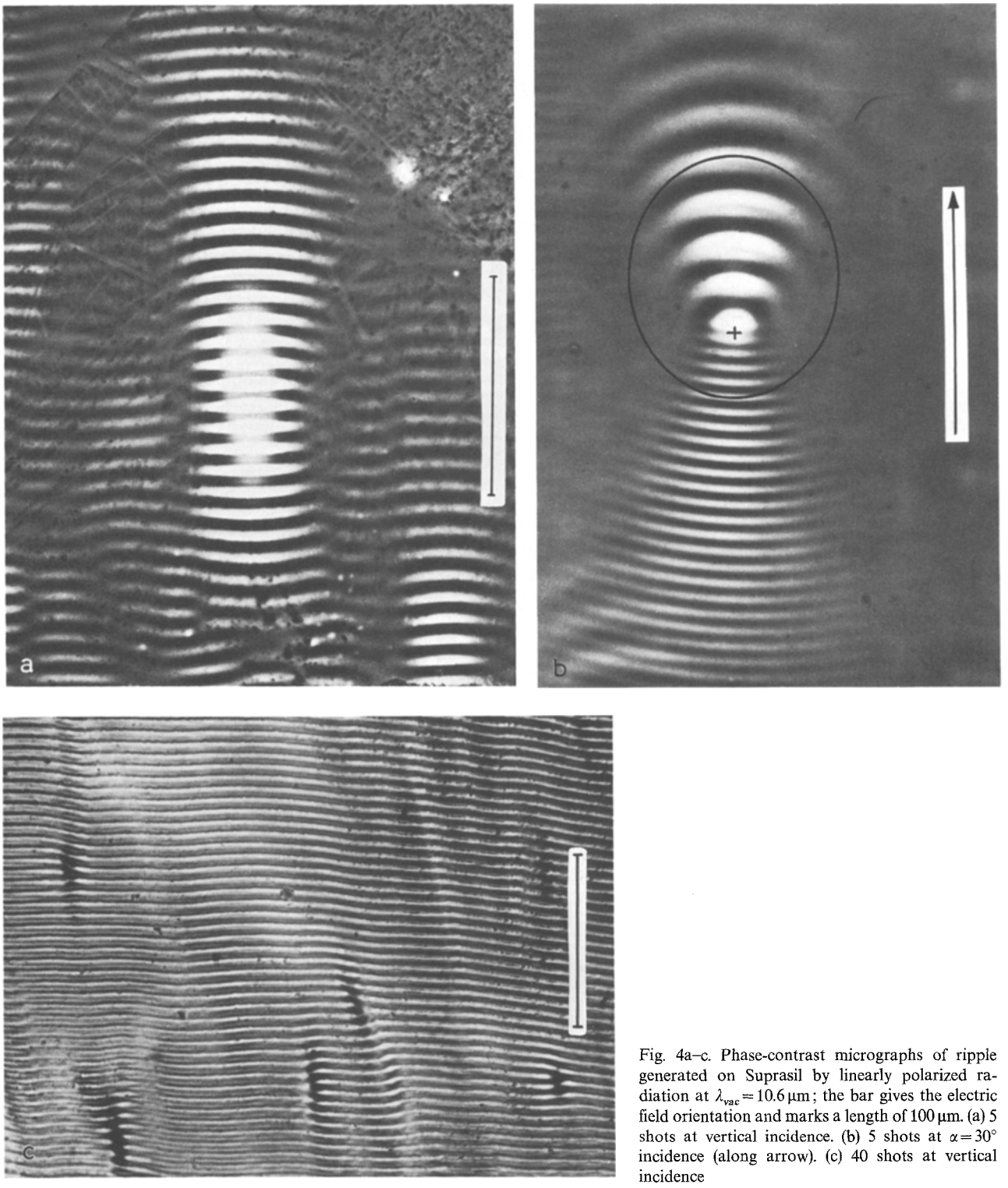

Fig. 4a–c. Phase-contrast micrographs of ripple generated on Suprasil by linearly polarized radiation at $\lambda_{vac} = 10.6\,\mu m$; the bar gives the electric field orientation and marks a length of 100 μm. (a) 5 shots at vertical incidence. (b) 5 shots at $\alpha = 30°$ incidence (along arrow). (c) 40 shots at vertical incidence

Slightly elliptic input polarization does not alter the picture: as seen in Fig. 7 the grooves remain perpendicular to the elongated axis of the polarization ellipse. The ripple amplitude however decreases with ellipticity and no hint of a periodic structure can be seen for circular polarization ($\alpha = 90°$), even for the doubled number of shots.

In Fig. 8 we summarize our results on ripple spacing as a function of incident wavelength. With $\lambda_{vac} = 10.6\,\mu m$ as in Figs. 4–7 the inverse ripple period exceeds the

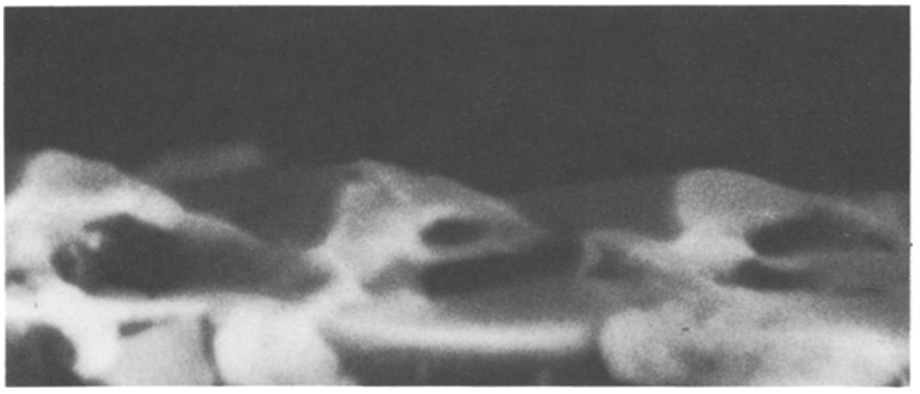

Fig. 5. Scanning electron micrograph of rippled surface of Fig. 4c. The glass sample was broken off at the bottom to give a three-dimensional visualization

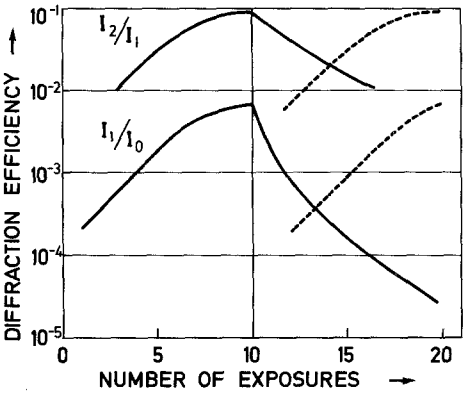

Fig. 6. Build-up and decay of ripple pattern on consecutive shots (Suprasil, $\lambda_{vac} = 10.6\,\mu m$, vertical incidence) measured by *s*-polarized He–Ne laser diffraction. After 10 shots the CO_2-laser polarization was changed by 90°; the dashed lines mark the appearance of the orthogonal ripple

laser wavenumber by 15% for the fully developed pattern, but only by 6% for the isolated wavetrains. Such a difference remains as with increasing frequency we find increasingly higher deviations from the vacuum light line. At the lower right of Fig. 8 five points mark the observation of even higher periodicity ripple weakly present simultaneously with the ordinary one. The isolated point marking a $3300\,cm^{-1}$ inverse ripple period is from the micrograph Fig. 9 which was found accidentally while using an electron microscope. At the higher frequencies orthogonally oriented ripples appear with periodicities left of the light line (Fig. 10). They dominate at the highest frequencies tried. Somewhat in contrast to the former cases they appear to be different on quartz and glass and show the same periodicity for isolated wavetrains and fully developed ripple pattern.

Finally at nonnormal incidence fully developed patterns show two periodicities which do not overlap spatially (Fig. 11). The results are shown in Fig. 12 for three wavelengths.

5. Discussion

We now interpret our results in terms of polariton interference. The data in Fig. 8 which are for normal incidence should then directly represent the surface polariton dispersion through the simple relation (1). For a flat surface the TM surface polariton dispersion branch extends between two limiting frequencies, ω_1 and ω_2 [13–15] which are given by the dielectric function of the material $\varepsilon'(\omega_1) = 0$ and $\varepsilon'(\omega_2) = -1$. To find these frequencies for hot quartz glass we use the data of [23] in Fig. 13. Taking 1100 °C, a temperature in the softening region, we obtain $\omega_1 = 1040\,cm^{-1}$ and $\omega_2 = 1120\,cm^{-1}$. The expected surface phonon polariton dispersion branch is sketched dashed in Fig. 8 [13–15]. No effects of damping have been included. Damping would imply a continuation of the curve into the radiative region on the left of the light line, and a shift to lower frequencies.

The data points on the right of the light line (Fig. 8) all fall below the expected dispersion curve, but tend to line up on shifted curves of similar shape. Since the periodicities of the fully developed structures are consistently larger than those of the isolated wavetrains, we infer that the dispersion curve shifts to the right with increasing ripple amplitude, i.e. that the surface wave phase velocity slows down due to the corrugation.

Surface wave propagation in the presence of corrugation is treated e.g. in grating theory [18, 24] and in waveguide studies e.g. [25]. Typically one has a fixed grating with wave vector **g** and studies the propagation as a function of frequency. Solutions result which contain spatial harmonics offset at wavevectors $N|\mathbf{g}|$ where N is an integer, similarly as with Bloch waves in a periodic crystal. Due to Bragg reflection forbidden gaps open up at surface wave vectors $(N/2)|\mathbf{g}|$ and parts of the dispersion curves become "radiative", i.e. $v_{ph} > c$.

The situation in our case (Fig. 8) is somewhat different. On varying the frequency, the grating vector **g** varies

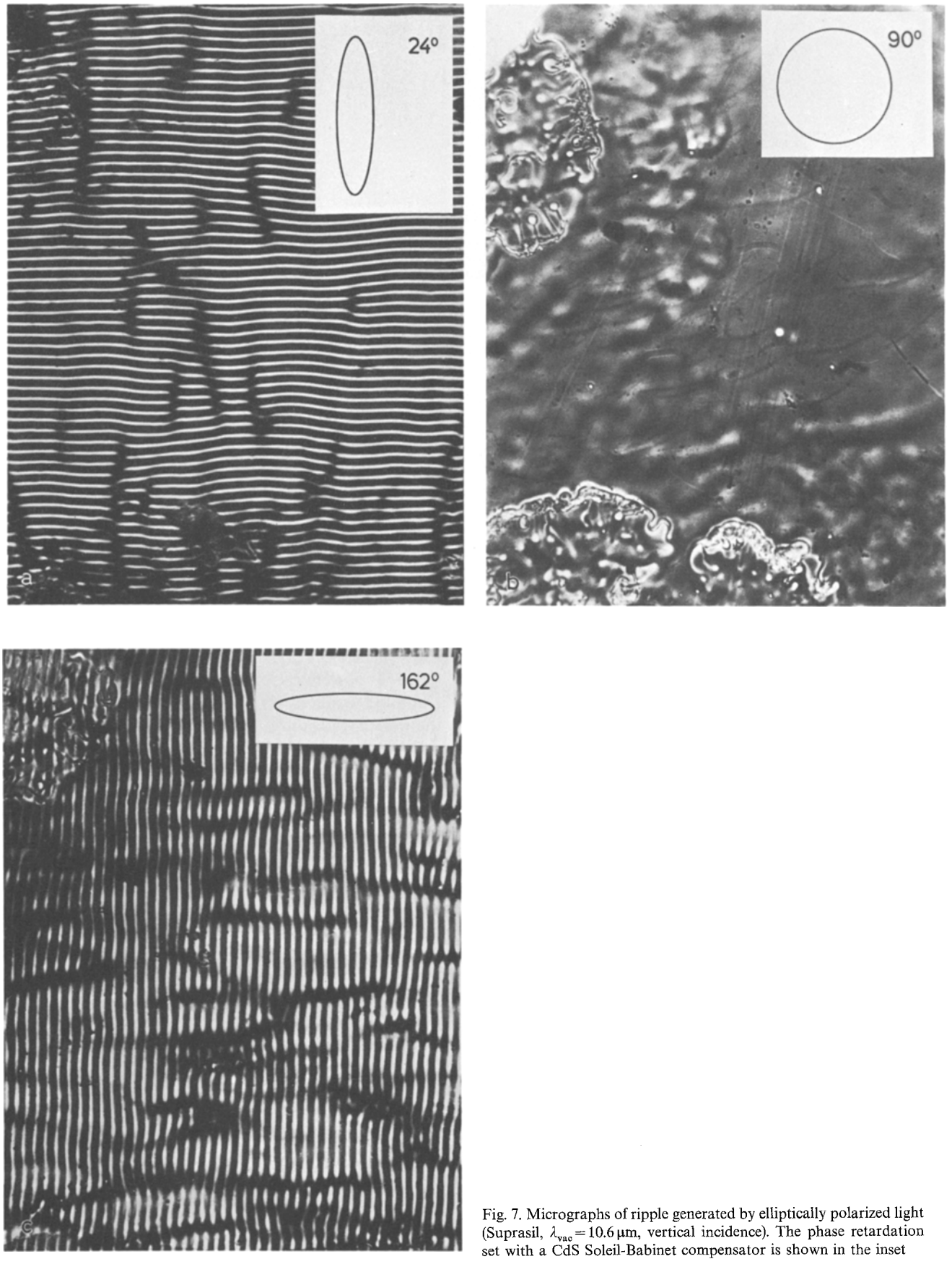

Fig. 7. Micrographs of ripple generated by elliptically polarized light (Suprasil, $\lambda_{vac} = 10.6\,\mu m$, vertical incidence). The phase retardation set with a CdS Soleil-Babinet compensator is shown in the inset

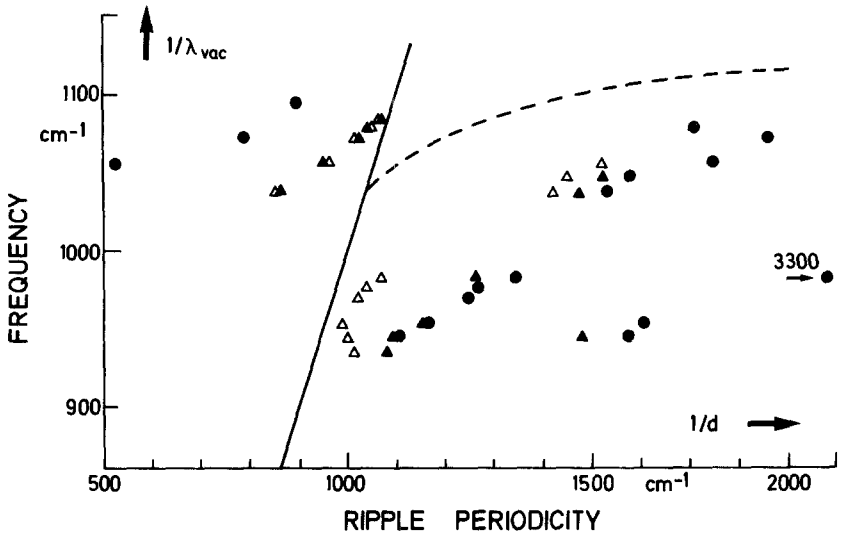

Fig. 8. Dependence of ripple periodicity $1/d$ on laser wavelength (linear polarization, vertical incidence). The straight line is given by $d=\lambda_{vac}$ ("vacuum light line"). All experimental points on the left and right of this line happen to correspond to grooves parallel and perpendicular, respectively, to the incident electric field. The symbols ● and ▲ mark measurements on fully developed patterns (Fig. 4c) on crystal quartz and Suprasil, respectively, using He–Ne laser scattering. △ stands for direct readings from Suprasil micrographs showing isolated wavetrains as in Fig. 4a. For the dashed curve see Sect. 5

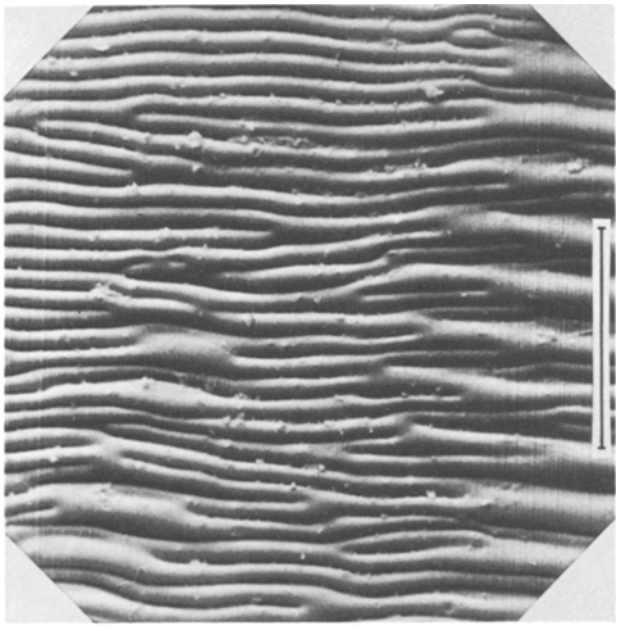

Fig. 9. Transition between normal and fine ripple regions on quartz observed with scanning electron microscope ($\lambda_{vac}=10.18\,\mu m$, vertical incidence, linear polarization with **E** along scale bar of length 30 μm)

according to (2). This means that the surface waves are tied to the Bragg resonance of the grating. The dispersion in such a situation has to our knowledge not been analyzed theoretically. There might be similarities to dispersion studies in distributed feedback lasers where however the emission frequency is the self-adjusting quantity in a fixed grating structure. It may be that the results for plasmons propagating on statistically rough surfaces are applicable to our case; increasing roughness amplitudes were found to slow down the phase velocity of the surface waves [26].

Apart from the experimental points in Fig. 8 discussed so far, the form of the isolated wavetrains as in Fig. 4a and b give us an independent observation of corrugation-induced slowing of quartz glass surface phonon polaritons. As is obvious from many such cases these structures originate in distinct centers often only a few micrometers in diameter, probably dust particles. Such centers emit approximately circular waves if we assume isotropic propagation. For non-normal incidence of the exciting light these give rise to a pattern of confocal elliptical interference fringes, with focus in the origin, as can be derived from (2). The major axis of the ellipse is parallel to the plane of incidence. In our experiment (Fig. 4b) observable fringe contrast is obtained only within an angular sector of approximately $\pm 20°$ from this axis. The reason for this is probably twofold: surface polaritons being TM polarized are (i) predominantly launched in the direction of the driving electric field and (ii) yield maximum interference contrast when propagating in this direction. A close inspection of patterns as in Fig. 4b reveal now that the fringes are not elliptical (we have inserted an ellipse with $\eta=0.48$ in Fig. 4b to illustrate this fact). Rather they seem to be ellipses deformed through compression along the major axis, by roughly 10%–20%. We believe this effect is due to the slowing of the surface polariton phase velocity due to the corrugation, an effect which is most prominent on axis, but nearly absent $\pm 20°$ away, where the corrugation vanishes.

The length of the wavetrains in Fig. 4a and b can be interpreted to yield the attenuation length of the surface polaritons. Note that two mechanisms contribute: dielectric absorption in the substrate and an interplay of radiative loss and gain mediated by the corrugation. The latter process decreases the fringe curvature and is responsible for the growth of the rippled area from shot to shot.

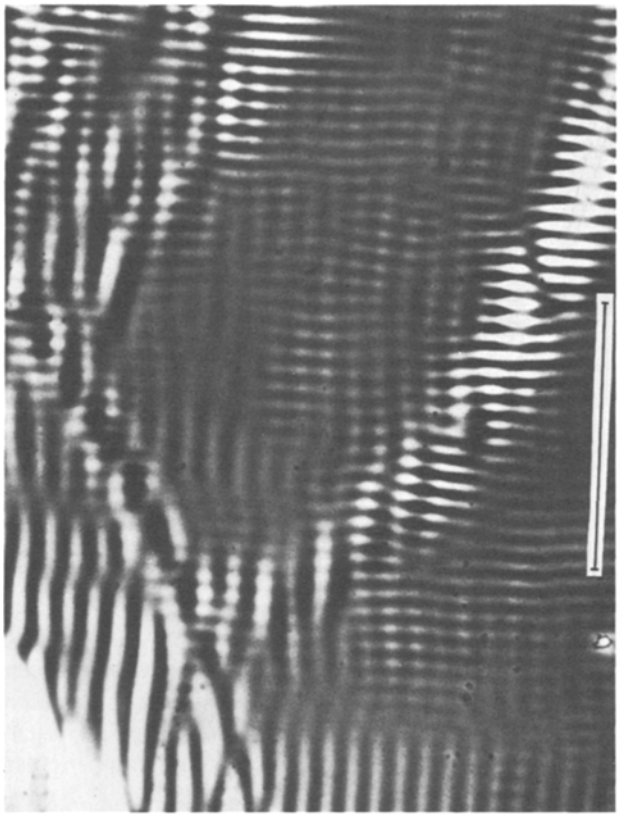

Fig. 10. Coexistence of orthogonally oriented ripple with spacings 6.6 and 10.6 μm on Suprasil ($\lambda_{vac} = 9.47$ μm, vertical incidence, linear polarization with **E** along scale bar of length 100 μm, phase contrast microscope)

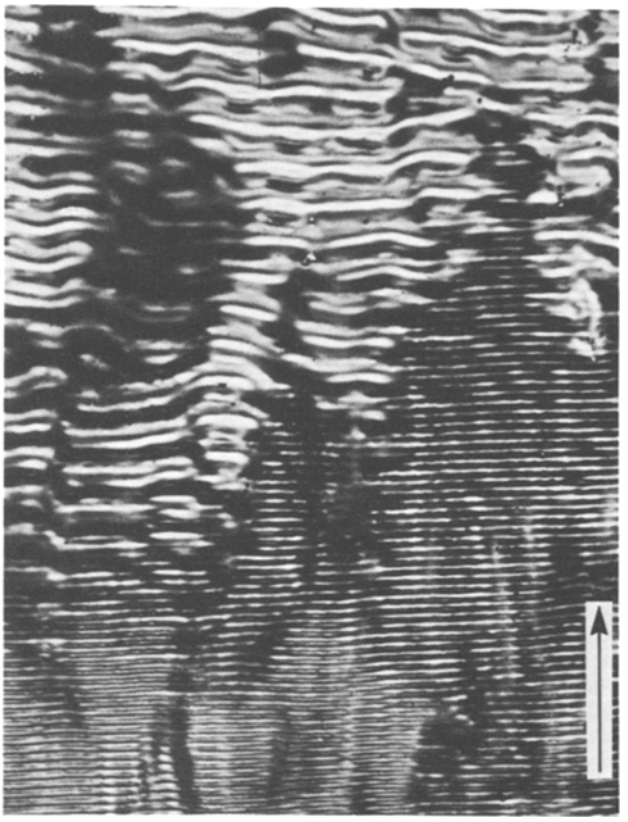

Fig. 11. Transition between "backward" and "forward" ripple regions on quartz resulting from *p*-polarized nonnormal laser incidence ($\lambda_{vac} = 10.27$ μm, incidence 18° from normal along arrow giving 100 μm scale)

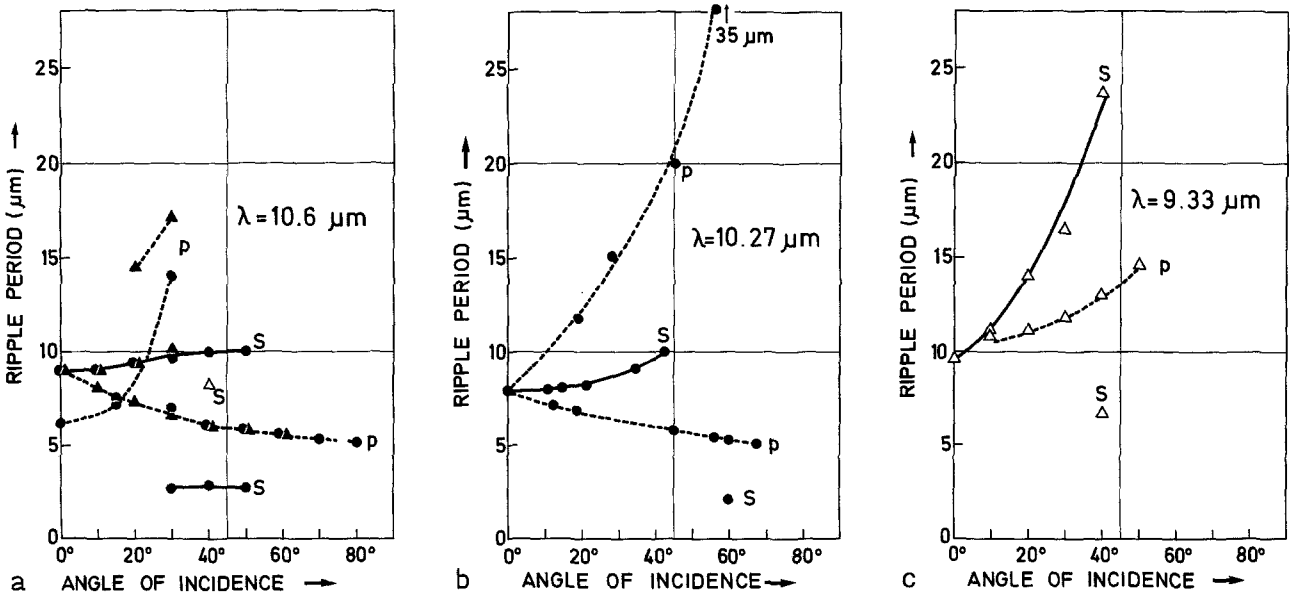

Fig. 12. Dependence of ripple period on angle of incidence. p and s denote linear input polarization with **E** parallel and perpendicular, respectively, to the plane of incidence. The symbols ● and ▲ mark grooves resulting perpendicular to **E**, for quartz and Suprasil, respectively. △ stands for Suprasil experiments where the grooves came out parallel to **E**. The connecting curves are drawn only to guide the eye

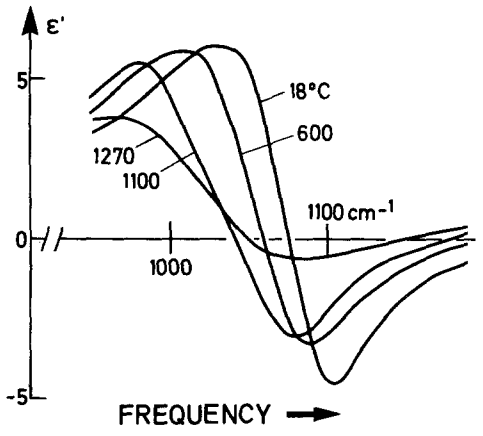

Fig. 13. Real part of dielectric constant of quartz glass [23] at different temperatures

Consider now the light scattering efficiency $\sigma = I_1/I_0$ (Fig. 6) which depends on both ripple amplitude and area. We find an initial increase by about a factor 1.8 per shot. When turning to orthogonal polarization, however, additional shots decrease σ by an even larger factor of 3.3 per shot. Loosely speaking we can therefore state that in the build-up phase there occurs during each shot a 70% erasure (due to melting) followed by a subsequent sixfold increase of the ripple strength (as measured by σ). Probably this competition between a loss and a gain process is responsible for our observation (Fig. 7b) that no ripple builds up with circular input polarization: while the loss factor equals the one in the linear case, a gain reduction by only a factor 2 suffices to result in a net gain factor smaller than 1. Such a reduction factor can be already expected for the decrease of interference contrast when using a circularly instead of a linearly polarized reference wave.

A further remark in this context can be made by inspection of fully developed patterns generated at oblique incidence. As is shown by Fig. 11 two possible ripple structures occupy domain-like areas with sharp boundaries. The two modes can be assigned to either forward scattering, with $0 < \alpha < \pi/2$ (Fig. 2), or to backward scattering with $-\pi/2 < \alpha < 0$. The periodicities observed then obey (1) with values of c/v_{ph} varying from 1.01 to 1.5 for all those cases of Fig. 12a and b where the ripple lines came out perpendicular to the plane of incidence. The strong dominance of one such mode in a given location is only understandable by invoking a partial erasure mechanism, as above, and a competition for gain between both modes. The latter is most probably brought about by partial depletion of the input wave once one of the ripple modes has reached high enough amplitude for efficient grating coupling.

The observations discussed so far fit our basic model of surface polariton interference, apart possibly from the exceptionally high periodicity point of $3300\,cm^{-1}$ in Fig. 8. It thus remains to discuss our observation of "extraordinary" ripple with lines parallel to the driving electric field. As seen in Fig. 10 these structures can spatially coexist with the ordinary ripple, indicating less mutual competition. We can not offer a definite model for the generation of these structures, but we can show that surface polaritons play a key role here as well. First the isolated wavetrains in these cases are very similar in shape to those, e.g., in Fig. 4a. With nonnormal incidence we obtain, for fully developed patterns, again two different ripple modes; the periodicities follow (1) with values c/v_{ph} varying now from 0.64 to 1.04 for those cases of Fig. 12a and c where the ripple lines came out perpendicular to the plane of incidence. Furthermore, the structures obtained at normal incidence have periodicities which form curves resembling dispersion branches (Fig. 8, left of light line).

The extraordinary ripple could therefore be explained by surface polariton interference if one could assume a surface polariton which has a transverse electric component in the surface. Theoretically, TE polarized surface polaritons can exist, e.g., when the dielectric constant of the material varies with depth [27]. Steep temperature gradients are surely present during ripple formation in our experiment. To give an idea of the depth involved, we state that the infrared penetration depth strongly decreases with frequency above $1000\,cm^{-1}$ for glass [22] and $1030\,cm^{-1}$ for quartz [21], and reaches $2\,\mu m$ at 1020 and $1050\,cm^{-1}$, respectively, for glass and quartz (all at room temperature). Still we can not explain why the extraordinary ripple periodicities fall left of the light line, i.e., why the TE surface polaritons should be leaky.

As the last case let us consider ripples generated with lines parallel to the plane of incidence. These are observed both for the ordinary and extraordinary mode. As seen in Fig. 12a–c the periods of these structures increase weakly with increasing angle of incidence. This can be quantitatively understood from our polariton interference model by use of (2) taking $\mathbf{g} \| y$ (Fig. 3) to obtain

$$d = \lambda_{vac}/[(c/v_{ph})^2 - \sin^2\alpha]^{1/2}. \quad (4)$$

6. Conclusions

The experimental results obtained establish the central role of surface polaritons in the ripple formation process on quartz. Support for our interference model comes from the dependences of the ripple periodicity on frequency, polarization and angle of incidence of

the driving laser beam. The resulting structures are strongly influenced by effects of surface corrugation on the surface wave dispersion which deserves further study.

Ripple formation via surface polariton interference can occur on a variety of sufficiently conductive materials, e.g., metals and semiconductors, if melting temperatures are reached. Even when only transiently present, ripples could be essential for enhanced coupling and absorption in laser processes like steel cutting [28] or plasma production [29].

The observation of interference of surface waves and a reference wave is a new tool for the study of surface polaritons. The advantage of this method is that for a given frequency both the real and the imaginary part of the surface polariton wave vector can be obtained from two simple length measurements. For this purpose we have developed photographic processes for the infrared and visible regions which are less perturbing than is ripple formation [30]. These methods can also be used to study the antenna properties of small particles or other structures on a flat surface, and more general, serve as a basic tool for a two-dimensional wave optics in the near infrared and visible regions.

Acknowledgements. We gratefully acknowledge stimulating discussions with L. Genzel, J. Lagois, E. Mohler (Frankfurt), A. A. Maradudin (Irvine), R. Ulrich (Hamburg), and E. Vinogradov (Moscow).

References

1. M. Siegrist, G. Kaech, F.K. Kneubühl: Appl. Phys. **2**, 45 (1973)
2. D.C. Emmony, R.P. Howson, L.J. Willis: Appl. Phys. Lett. **23**, 598 (1973)
3. C.T. Walters: Appl. Phys. Lett. **25**, 696 (1974)
4. L.J. Willis, D.C. Emmony: Opt. Laser Technol. (Oct. 1975) p. 222
5. N.R. Isenor: Appl. Phys. Lett. **31**, 148 (1977)
6. H.J. Leamy, G.A. Rozgony, T.T. Sheng: Appl. Phys. Lett. **32**, 534 (1978)
7. M. Oron, G. Sorensen: Appl. Phys. Lett. **35**, 782 (1979)
8. A.K. Jain, V.N. Kulkarni, D.K. Sood, J.S. Uppal: J. Appl. Phys. **52**, 4882 (1981)
9. P.A. Temple, J.J. Soileau: IEEE J. QE-**17**, 2067 (1981)
10. J.C. Koo: Appl. Phys. Lett. **28**, 614 (1976)
11. C. Hill, D.J. Godfrey: J. Phys. (Paris) **41** Suppl. 5, C4-**79** (1980)
12. G.N. Maracas, G.L. Harris, C.A. Lee, R.A. McFarlane: Appl. Phys. Lett. **35**, 453 (1978)
13. A. Otto: Optik **38**, 566 (1973)
14. E. Burstein, W.P. Chen, Y.J. Chen, A. Harstein: J. Vac. Sci. Technol. **11**, 1004 (1974)
15. A.A. Maradudin: In *Festkörperprobleme*, Vol. 21, ed. by J. Treusch (Vieweg, Braunschweig 1981) pp. 62–116
16. A. Otto: Z. Physik **216**, 398 (1968)
17. P.K. Tien, R. Ulrich, R.J. Martin: Appl. Phys. Lett. **16**, 198 (1970)
18. R. Petit (ed.): *The Electromagnetic Theory of Gratings*, Topics Current Phys. **22** (Springer, Berlin, Heidelberg, New York 1980)
19. H. Haken, H. Sauermann: Z. Physik **173**, 261 (1963)
20. W.E. Lamb: Phys. Rev. **134**, 1429 (1964)
21. W.G. Spitzer, D.A. Kleinmann: Phys. Rev. **121**, 1324 (1961)
22. T.R. Steyer, K.L. Day, D.R. Huffmann: Appl. Opt. **13**, 1586 (1974)
23. N. Neuroth: Z. Physik **144**, 85 (1956)
24. B. Laks, D.L. Mills, A.A. Maradudin: Phys. Rev. B**10**, 4965 (1981)
25. R. Ulrich: In *Optical and Acoustical Micro-Electronics*, ed. by J. Fox, Mic. Res. Symp. Series, Vol. 23 (Polytechnic Press, New York 1974) pp. 359–376
26. H. Raether: In *Physics of Thin Films*, Vol. 9 (Academic Press, New York 1977) pp. 145–261
27. H.M. Barlow, J. Brown: *Radio Surface Waves* (Clarendon Press, Oxford 1962)
28. F.O. Olsen: 5th Int. Congr. "Laser 81", Munich (1981)
29. D.M. Villeneuve, G.D. Enright, M.C. Richardson, N.R. Isenor: J. Appl. Phys. **50**, 3921 (1979)
30. F. Keilmann: In preparation
31. H. Nassenstein: Phys. Lett. **28**A, 249 (1968)
32. J.J. Cowan: Opt. Commun. **5**, 69 (1972)
33. T. Suhara, H. Nishira, J. Koyama: Opt. Commun. **19**, 353 (1976)

Note added in proof: Interference patterns of inhomogeneous optical waves have been observed before, in cases of Brewster waves [31], surface plasmon polaritons [32] and also guided slab waves [33]. We are indebted to G.T. Sincerbox (San José) for bringing these references to our attention.